Photoinitiation study of Irgacure 784 in an epoxy resin photopolymer

Dušan Sabol, Michael R. Gleeson, Shui Liu, and John T. Sheridan[a)]
UCD Communications and Optoelectronic Research Centre, SFI Strategic Research Cluster in Solar Energy Conversion, School of Electrical, Electronic and Mechanical Engineering, College of Engineering, Mathematical and Physical Sciences, University College Dublin, Belfield, Dublin 4, Republic of Ireland

(Received 7 July 2009; accepted 19 November 2009; published online 12 March 2010)

A deeper understanding of the processes, which occur during free radical photopolymerization, is necessary in order to develop a fully comprehensive model, which represents their behavior during exposure. One of these processes is photoinitiation, whereby a photon is absorbed by a photosensitizer producing free radicals, which can initiate polymerization. These free radicals can also participate in polymer chain termination (primary termination), and it is therefore necessary to understand their generation in order to predict the temporally varying kinetic effects present during holographic grating formation. In this paper, a study of the photoinitiation mechanisms of Irgacure 784 photosensitizer, in an epoxy resin matrix, is presented. We report our experimental results and present a theoretical model to predict the physically observed behavior. © *2010 American Institute of Physics*. [doi:10.1063/1.3276173]

I. INTRODUCTION

In the literature, extensive research is currently being carried out on a variety of photopolymer materials. Their inexpensive, self-processing capability and low loss make them promising materials for a variety of applications.[1–12] In order to reach their full potential, accurate material models based on reproducible experimental data sets will be necessary. In particular, such models are needed to identify and permit optimization of crucial operational parameters.

In this paper we focus on the photoinitiation processes, which take place in such materials during exposure. These processes begin with photon absorption by a photosensitizer leading to free radical generation. The resulting free radicals can react with (i) monomer, initiating growth of polymer chains and therefore changes in refractive index, (ii) inhibitors, being scavenged, or with (iii) monomer radicals, thus terminating a polymer active tip.

Photosensitizer consumption reduces the absorbance of a photopolymer layer. Thus the number of free radicals produced can be estimated by measuring the temporal variation of the transmitted light through the photopolymer layer (transmission curve). In this paper we study the case of a photoinitiator where photodissociation (photocleaving) generates chemical by-products that absorb at the green exposing wavelength ($\lambda = 532$ nm). This additional absorption during exposure can lead to an inaccurate estimate of the rate of production of free radicals. Therefore, photon absorption arising due to the presence of such inactive photoinitiation species (noninitiating) must be understood. In order to separate the effects of multicomponent absorption we introduce an additional red probe ($\lambda = 633$ nm) laser beam, which does not affect the exposing green driven photoinitiator photodissociation but is attenuated by the resulting intermediate by-products. A decrease in the output intensity of the red probe beam then provides information about the absorptivity of the intermediate by-products at the green exposing wavelength. In this way we can extract quantitative information about both the inactive by-products and the photoinitiator.

Photopolymerization processes play an important role in polymer chemistry. Photopolymerization can be achieved by two different processes: (a) one photon absorption for each propagation step, i.e., *direct photopolymerization*, or (b) the more efficient *photoinitiated polymerization*, which requires the absorption of just one photon for the production of a chain initiator species (i.e., activation step).[3,13] This second system contains at least two components: a photoinitiator and a polymerizable material.[3,4] Once the photoinitiator has produced a chain initiator species, polymer formation occurs by nonphotochemical propagation reactions of free radicals, cations, or anions.[13] Numerous optical components are commonly produced using materials which undergo free radical photopolymerization,[2] and they are also widely studied as an optical data storage media.[4–11]

Free radical photopolymerization can be initiated either by the reaction of an excited state photosensitizer dye with a coinitiator, e.g., an electron donor or an electron acceptor, producing free radicals, or by direct photocleavage of the photoinitiator molecule.[3,14] Useful photoinitiator systems have to meet a few basic requirements: (i) The photoinitiator system and polymerizable material must be thermally stable, (ii) they should exhibit strong absorption in the wavelength region of interest, and (iii) they should efficiently produce free radicals in order to start polymerization.[3] We analyze a system, which meets all of these requirements.[8]

This paper is divided into six sections. In Sec. II we describe the photopolymer material composition and the preparation procedure used. In Sec. III we describe in detail the photoinitiator used, the organometallic titanocene compound Irgacure 784, its chemical properties, possible photochemical reactions, and photoproducts. A flowchart summarizing all the reactions considered to take place during exposure is provided. Section IV is divided into three sub-

[a)]Author to whom correspondence should be addressed. Electronic mail: john.sheridan@ucd.ie. Tel.: +353-1-716-1927. FAX: +353-1-283-0921.

TABLE I. Epoxy resin photopolymer material composition.

Function	Compound	Acronym	Mass (g)
Matrix	Poly(propylene glycol) diglycidyl ether	PGE	10.000
	Diethylenetriamine	DTA	2.1900
Writing monomers	1-vinyl-2-pyrrolidone	NVP	0.9125
	9-vinylcarbazole	NVC	0.9125
Photosensitizer	Irgacure 784	A	0.6140
Inhibitor	2,6-di-tert-butyl-4-methylphenol	BHT	0.0068

sections. Section IV A deals with the modeling of the photochemical processes described in Sec. III. In Sec. IV B the predictions made using the model derived in Sec. III, for three different exposing intensities, are presented and discussed. In Sec. IV C the experimental setup and the experiments performed to analyze the photoinitiator are described. In Sec. V we discuss the numerical procedure used to extract key material parameters by fitting the experimental data for different exposure intensities. The best fits are found by minimizing a cost function, i.e., the root mean square error (RMSE). Finally, we summarize our results and present our conclusions in Sec. VI.

II. MATERIAL COMPOSITION

Our photopolymer material consists of (a) two very different polymerizable systems, (b) a photoinitiator, and (c) an inhibitor. This type of material was originally proposed by Trentler *et al.*[8] It has several practical advantages including its ability to be cast into large stable layer thicknesses and to record high refractive index modulations. The *first polymerizable system* is made of a combination of a low refractive index epoxy resin matrix, poly(propylene glycol) diglycidyl ether ($n=1.464$), and an amine hardener, diethylenetriamine ($n=1.484$). They are selected to have high transparency, low refractive indices, and minimal chemical interaction with the other compounds present, e.g., the writing monomers and photoinitiator. After mixing, the matrix components spontaneously crosslink with each other at room temperature and form a rigid mesh structure (the matrix). This cured epoxy resin matrix accommodates all components in a mechanically and environmentally stable way. The *second polymerizable system* is a mixture of two high refractive index vinyl monomers: 1-vinyl-2-pyrrolidone ($n=1.51$) and 9-vinylcarbazole ($n=1.68$). These monomers react via free radical photopolymerization to form polymer chains. Free radicals are produced following absorption by a *photoinitiator system* involving, in this case, an organometallic titanocene, Irgacure 784. This photoinitiator undergoes photocleaving after photon absorption.

This basic composition may be extended by introducing other chemicals, for example, terminators, chain transfer agents,[6,15] reducing agents,[8] etc. In the material composition examined here we add an *inhibitor*, 2,6-di-tert-butyl-4-methylphenol, whose purpose is to stop undesired spontaneous polymerization before exposure, i.e., dark reactions. All chemical components, acronyms, and the compositional weights used in this paper are listed in Table I.

This type of material design permits the recording of high refractive index modulations in mechanically stable layers, which can be cast to large thicknesses. The material (dry layer) preparation procedure is as follows:

(1) The required weights of each component are placed into a 100 ml beaker. The photosensitizer is added last and, following its inclusion, every step is performed under dark conditions, i.e., in red light.
(2) The mixture is heated and gently stirred at 50 °C for approximately 20 min.
(3) The composition is cooled down and placed into a bell jar and vacuum pumped for approximately 1.5 h to remove air and other gases.
(4) Material is then drawn into a syringe while the viscosity is still low. It is then necessary to wait until it has optimal consistency. Viscosity must be high enough to prevent the free flow of the material over the glass substrate. On the other hand it must be low enough to adhere to the glass and allow any air bubbles present to emerge from the layer.
(5) On the microscope glass slide, of size 26×76 mm^2, plastic spacers of the desired layer thickness are positioned. Then an appropriate volume of material with suitable viscosity is drop cast. The material is carefully covered by a second glass slide to avoid trapping air bubbles. A weight is applied to the top slide to ensure the uniform spread of material before hardening.
(6) Samples are laid out to cure for at least 6 h. They are stored in the dark at room temperature.

The layers are now ready for use. The photochemical reactions are discussed in Sec. III.

III. THE CHEMISTRY OF PHOTOINITIATION

As stated in Sec. II the photopolymer contains the photoinitiator Irgacure 784, which does not require an electron donor in order to produce free radicals.[16] Its chemical structure is described in detail in Refs. 10, 14, and 17.

The decompositions, i.e., photocleaving, which take place due to illumination, of several different titanocene photoinitiators, including Irgacure 784, have been studied in literature and several possible reaction paths have been proposed.[3,10,14,17–20] In this study we follow Ref. 19 and assume that isomerization takes place before the photocleaving of the generated isomer. Therefore, we assume the existence of two absorptive intermediate products: an isomer and a

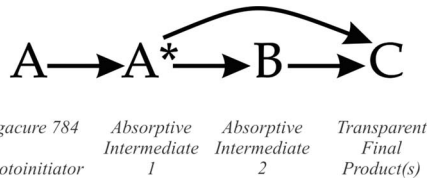

FIG. 1. Proposed reaction path, or cascade of photochemical reactions.

photocleaved isomer, which both eventually react to form stable transparent products. These processes are illustrated in Fig. 1.

The capital letters in Fig. 1 (**A**, **A***, **B**, and **C**) represent the chemical component taking part in the photoinitiation process. "**A**" and "**A***" represent Irgacure 784 and its isomer, respectively, "**B**" is an unstable intermediate arising after photocleaving, and "**C**" represents all stable transparent end products.

Let us now describe in greater detail the previously outlined processes. The absorption of light quanta by a molecule of Irgacure 784, **A**, causes reversible isomerization where one η^5-cyclopentadien-1-yl compound (Cp) converts to the η^1-cyclopentadien-1-yl form

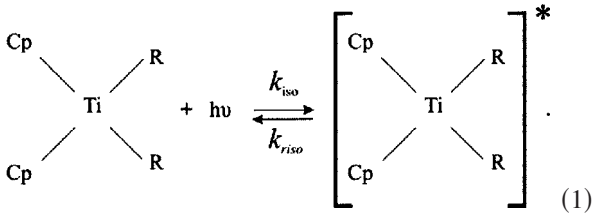

(1)

The initial form of Irgacure 784, **A**, appears as a reactant on the left side of Eq. (1) and its isomer, **A***, appears on the right. This new isomer has a different absorption spectrum and with time can either return to the original, **A**, form through reverse isomerization, which takes place at a rate k_{riso}, or can photocleave, at a rate k_B, to create an unstable titanocene diradical, **B**, and a stable aryl compound, as presented in Eq. (2)

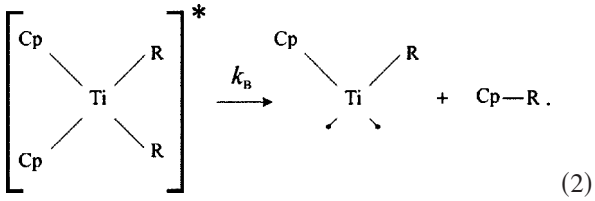

(2)

Another possible reaction that can take place is the removal of the isomer **A*** at a rate k_C to form the stable transparent product, **C**. It is speculated that the mechanism, by which this takes place, may involve some reaction or interaction with another reactant, e.g., one of the matrix components.[19] The photocleaved absorptive diradicals produced in Eq. (2) can react to form a stable transparent state through reaction with a reducing agent. All the reactions and the states considered in this model are summarized in the flowchart presented in Fig. 2.

It must be emphasized that **C** is, in fact, generated by at least two contributions: (i) the reaction of the isomer and (ii) the reaction of the diradical. These contributions are not necessarily identical in terms of their chemical structure, but they are both assumed to be completely transparent at both the exposing and probing wavelengths.

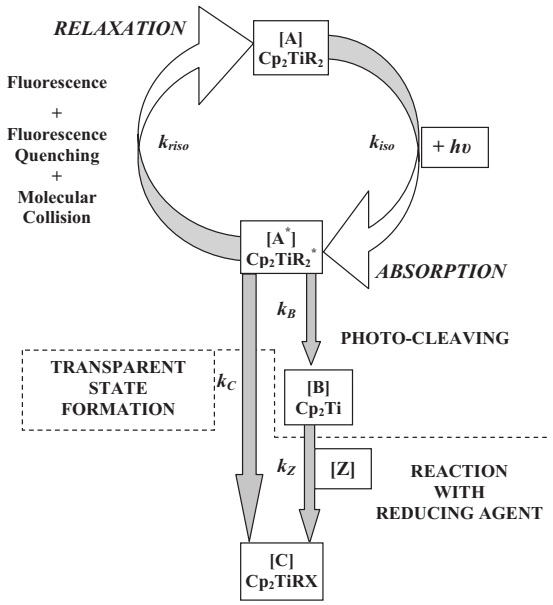

FIG. 2. Photochemical flowchart for Irgacure 784.

In this section we have discussed the properties of the photoinitiator and our assumptions regarding the photochemical processes, which take place during exposure. In Sec. IV we derive a mathematical model based on the proposed reactions.

IV. MODELING PHOTOINITIATION

In Sec. III we presented the chemical equations, which we assume govern the photoinitiation processes, which occur in the epoxy resin photopolymer under examination. We wish to predict the temporal evolution of the molar concentrations of each component during exposure. These concentration values, in conjunction with the molar absorption coefficients, and the fraction of light transmitted through the photopolymer layer (transmission curve), will allow us to estimate the amount of light absorbed by each individual component present.

A. Rate equations

We begin by assuming that the variations of the transmitted intensity with time, $I(t)$, are solely due to the changes in the various absorber concentrations, which are uniformly spatially distributed in the photopolymer layer. This allows us to describe the temporal evolution of transmittance, $T(t)$, using

$$T(t) = T_{\mathrm{SF}} \frac{I(t)}{I_0} = T_{\mathrm{SF}} \exp\left[-\sum_{m=1}^{M} \varepsilon_m c_m(t) \frac{d}{\cos\,\theta} \right], \tag{3}$$

where I_0 is the input intensity, ε_m and c_m are the molar absorption coefficient and the molar concentration (of the m^{th} of M absorbers) at time t, d is the layer thickness, and θ is the angle of incidence to the normal inside the layer. T_{SF} is a

loss fraction, which takes account of Fresnel and scatter losses at the boundaries.[5,6]

Initially the only absorber present is the photoinitiator, **A**, whose concentration is fixed by the material composition. The initial concentrations of all the other absorbers are zero. As we expose the layer, the photoinitiator and photoproduct concentrations change. As shown later, these changes can be modeled using first-order coupled differential equations; see Eqs. (4)–(8).

Equation (4) includes the two processes, which lead to a variation in the concentration of Irgacure 784, $A(t)$. First, the removal of this photosensitizer due to absorption, and second the recovery back to the initial state, **A**, from the isomeric state, $\mathbf{A}^*$.

$$\frac{dA(t)}{dt} = -\frac{k_{\text{iso}}}{d} I^{532}(t) A(t) + k_{\text{riso}} A^*(t), \tag{4}$$

where $I^{532}(t)$ is the number of transmitted green ($\lambda = 532$ nm), exposing photons in Einstein/cm^2, available to be absorbed by Irgacure 784, i.e., $A(t)$ in mol/cm^3. This removal occurs at the rate k_{iso} divided by the thickness of the layer d in centimeter.[21,22]

The removal term in Eq. (4) leads to the production of the isomer concentration $A^*(t)$ in

$$\frac{dA^*(t)}{dt} = \frac{k_{\text{iso}}}{d} I^{532}(t) A(t) - A^*(t)(k_{\text{riso}} + k_B + k_C). \tag{5}$$

This isomer then reacts and is consumed in *three* possible ways: (1) At first, it undergoes recovery, or reverse isomerization, to the initial state **A** at a rate k_{riso}. This term appears in both Eqs. (4) and (5), and is less significant for short exposure times compared to the fast acting removal term in Eq. (4). The other possible reactions then occur at two specific rates k_B and k_C: (2) isomer photocleaving and creating the unstable absorptive intermediate $B(t)$ [see Eq. (6)], and (3) isomer conversion to the stable transparent product $C(t)$; see Eq. (7).

$$\frac{dB(t)}{dt} = k_B A^*(t) - k_Z B(t) Z(t). \tag{6}$$

The intermediate $B(t)$ is being removed in Eq. (6) through a reaction with the reducing agent $Z(t)$ at a rate k_Z, generating a stable transparent product $C(t)$ in

$$\frac{dC(t)}{dt} = k_C A^*(t) + k_Z B(t) Z(t). \tag{7}$$

The reducing agent $Z(t)$ is consumed by this reaction and therefore its concentration decreases as described in

$$\frac{dZ(t)}{dt} = -k_Z B(t) Z(t). \tag{8}$$

We note that in this analysis the possible effects of photoinitiator diffusion have been assumed to be negligible during exposure due to the large molecular weight (MW = 534.4 g/mol) and complex structure of the Irgacure 784 molecule. The solution of Eqs. (4)–(8) provides the time varying concentrations of the absorbing species. These can then be used in conjunction with their molar absorption coefficients, as in Eq. (3), to estimate the transmittance for normally incident exposing green light.

$$T^{532}(t) = T_{\text{SF}} \frac{I^{532}(t)}{I_0^{532}} = T_{\text{SF}} \exp\{-[\varepsilon_A{}^{532} A(t) + \varepsilon_{A^*}{}^{532} A^*(t) + \varepsilon_B{}^{532} B(t)]d\}. \tag{9}$$

This equation governs the temporal evolution of the transmitted intensity during exposure. Measuring the transmitted intensity of the exposing beam alone does not provide sufficient information to allow us to estimate the concentrations of three temporally varying absorbing species. Therefore it is necessary to perform other measurements in order for all the unknowns to be estimated.

In Sec. IV B we examine the predictions of the proposed model for various exposing intensities.

B. Simulated transmission curves

In Sec. IV A we proposed a photochemical model to describe the temporal evolution of the Irgacure 784 photoinitiator and the concentrations of its photoproducts, arising due to illumination by a green exposing beam. The rate of photoinitiator removal depends primarily on the fraction of the exposing intensity absorbed by the photoinitiator. Initially $A(0) = 1.04 \times 10^{-4}$ mol/cm^3 and $A^*(0) = B(0) = C(0) = 0$; therefore photon absorption occurs exclusively due to the photoinitiator, $A(t=0)$, resulting in maximum photoinitiator removal. This removal generates absorptive photoproducts, which then also absorb the available exposing photons; thus the rate of photoinitiator removal decreases. The amount of exposing light absorbed by the photoinitiator and the photoproducts depend on their concentrations and molar absorption coefficients. The values of the molar absorption coefficient for Irgacure 784 can be found from its absorption spectrum,[17] $\varepsilon_A{}^{532} = 1.2 \times 10^5$ cm^2/mol. The values used for the isomer $\mathbf{A}^*$, $\varepsilon_{A^*}{}^{532} = 1.3 \times 10^5$ cm^2/mol, and photocleaved intermediate **B**, $\varepsilon_B{}^{532} = 4.3 \times 10^4$ cm^2/mol, are chosen in order to resemble the reported behavior.[23]

Equations (4)–(9) can then be solved for some physically acceptable parameter values. These parameter values include the following: (i) The rates of photoinitiator removal and isomer production used are $k_{\text{iso}} = 4.8 \times 10^4$ cm^3 Einstein^{-1} s^{-1}, and we neglect reverse isomerization (recovery), i.e., $k_{\text{riso}} = 0$ s^{-1}. (ii) The rate of photocleaved intermediate **B** production used is $k_B = 0.035$ s^{-1}. (iii) The direct rate of production of the transparent **C** product from $\mathbf{A}^*$ used is $k_C = 0.015$ s^{-1}. (iv) An indirect rate of production of the transparent **C** product, through reaction of the reducing agent Z with **B**, of $k_Z = 1.1 \times 10^8$ cm^3/(mol s). Finally, (v) we assume an initial Z concentration of $Z(0) = 3.4 \times 10^{-7}$ mol/cm^3. We discuss the physical values used to solve Eqs. (4)–(8) in greater detail in Sec. V. For now, we proceed to simulate the transmittance $T^{532}(t)$ during exposure for three exposing intensities $I_0{}^{532}$ (16, 32, and 132 mW/cm^2). The resulting predictions are presented in Fig. 3.

In all three transmission curves appearing in Fig. 3, a significant increase in the intensity of the transmitted light is seen following long exposures. As expected the same maxi-

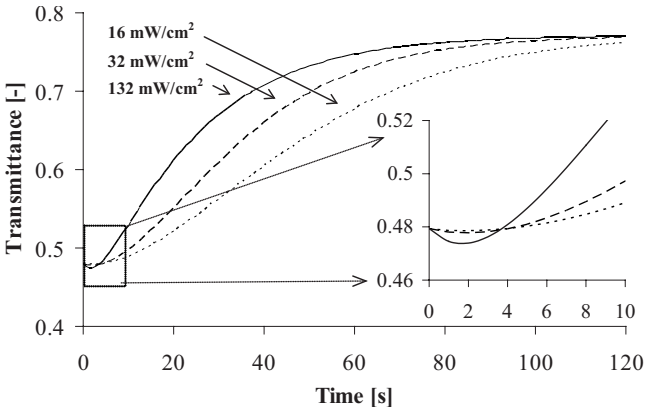

FIG. 3. Simulation of the transmission curves for three different exposing intensities, 16 (short-dashed), 32, (long-dashed) and 132 mW/cm^2 (solid line).

mum transmitted value is achieved but after different exposing times. Now, focusing on the initial period of exposure (see the inset in Fig. 3), we notice two different types of behavior. For the lower intensity cases, 16 and 32 mW/cm^2, we see a negligible change in the initially transmitted light during the first 4 s. However, at higher intensities, i.e., 132 mW/cm^2, the transmitted intensity decreases initially but then grows at a steep rate. We propose that this may occur when there is sufficient production and accumulation of the absorptive intermediate state, isomer $\mathbf{A}^*$, if $\varepsilon_{A^*}{}^{532} > \varepsilon_A{}^{532}$. We note that the behavior predicted here for higher exposing intensities, i.e., the initial decrease in the transmitted light, was previously observed in Ref. 23.

In this section, we have made a series of predictions regarding the behavior of Irgacure 784. We have demonstrated the ability of our model to predict results in agreement with experimental trends observed to take place for higher exposing intensities.[23] In Sec. IV C we describe our experimental method for studying this photoinitiation process.[7,21]

C. Experimental method

As noted in the Sec. III, we have assumed that the photodissociation of Irgacure 784 involves the production of two species both of which absorb at the exposing wavelength resulting in a slowing of the removal of the photoinitiator. We propose to monitor the absorption due to the production of the absorptive intermediates by introducing a red probe laser, $\lambda = 633$ nm, with a wavelength outside the region of sensitivity of the photoinitiator. Therefore the probe light will not be absorbed by the photoinitiator, but can be absorbed by the absorptive intermediates. The intensities of both the transmitted exposing and probe beams are simultaneously monitored during exposure. Any decrease in the measured probe transmitted intensity will solely depend on the concentrations and the molar absorption coefficients of the generated photoproducts. Therefore the probe beam transmittance can be given by

$$T^{633}(t) = T_{\mathrm{SF}} \frac{I^{633}(t)}{I_0{}^{633}} = T_{\mathrm{SF}} \exp\left\{ -\left[\varepsilon_{A^*}{}^{633} A^*(t) + \varepsilon_B{}^{633} B(t)\right] \frac{d}{\cos\theta} \right\}. \quad (10)$$

As the molar absorption coefficient of a species is a function of the wavelength, it can vary significantly depending on the wavelength used to measure them. The proposed experiment does not allow us to simply and unambiguously separate the values of the photoproduct concentrations and their molar absorption coefficients. However, their product, i.e., the optical density, can be determined. By performing this experiment with two wavelengths, we can find the ratio between the two molar absorption coefficients at these particular wavelengths. The individual concentration must then be separately measured, by means of an analytic chemical measurement (which would be cumbersome and require destruction of the layer), or estimated numerically by combining and applying a robust material model and a nonlinear fitting algorithm. In order to perform such a numerical estimation procedure detailed *a priori* knowledge must be available, including knowledge of the experimental conditions, i.e., the exposing intensities, the layer thicknesses, the photoinitiator concentration, etc. Furthermore, the models and fitting must be applied appropriately. Below we explore the use of Eqs. (4)–(10) to extract parameter values in this way.

The wavelength dependent absorption characteristics of Irgacure 784 are well documented.[17] It absorbs strongly from the UV region up to ~560 nm, and is transparent at longer wavelengths.[14] In our experiments we expose using a diode-pumped solid-state green laser, operating at a wavelength of 532 nm.

As stated, we propose that two absorbing species are generated during the exposure: the isomer of Irgacure 784 ($\mathbf{A}^*$) and its photocleaved product ($\mathbf{B}$). Both of which tend to react to form stable transparent forms ($\mathbf{C}$). We might reasonably expect $\mathbf{A}^*$ to have quite a similar absorption at the exposing wavelength 532 nm as $\mathbf{A}$, since it contains the same constituent atoms with one modified chemical bond, i.e., one η^1-cyclopentadien-1-yl and one of η^5-cyclopentadien-1-yl group instead of two η^5-cyclopentadien-1-yl groups. This result was confirmed for a similar titanocene photoinitiator.[19] This new (weaker) chemical bond in $\mathbf{A}^*$ is susceptible to photocleaving. Therefore we assume that $\mathbf{A}^*$ absorbs at both the exposing and probing wavelengths, and that $\varepsilon_{A^*}{}^{532} > \varepsilon_A{}^{532}$. We also assume that the molar absorption of $\mathbf{A}^*$ at the probing wavelength is small when compared to its value at the exposing wavelength, i.e., $\varepsilon_{A^*}{}^{532} > \varepsilon_{A^*}{}^{633}$. Thus we conclude that any observed decrease in the transmitted probe beam intensity is exclusively due to $\mathbf{A}^*$ (with $\varepsilon_{A^*}{}^{633}$) and $\mathbf{B}$ (with $\varepsilon_B{}^{633}$), since we assume $\varepsilon_A{}^{633} \approx 0$ cm^2/mol.

Irgacure 784 absorbs negligibly at wavelengths greater than 560 nm;[14] therefore a probe He–Ne laser of wavelength 633 nm was conveniently chosen. The transparency at this wavelength, i.e., the insensitivity of $\mathbf{A}$, was verified experimentally by probing an unexposed photopolymer layer for

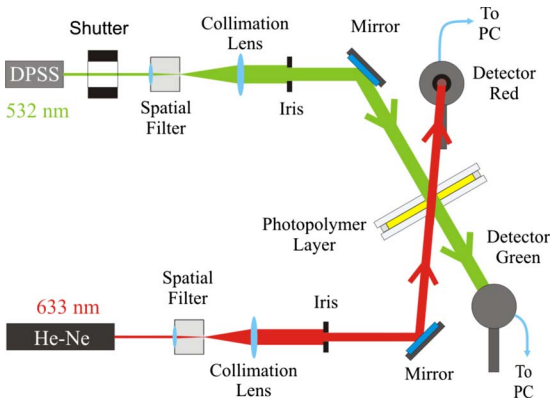

FIG. 4. (Color online) The experimental setup to measure transmittance curves of the green (532 nm) (exposing) and red (633 nm) (probe) beams.

durations longer than the exposure times used. In all cases the transmitted probe beam intensity was continuously monitored and remained constant.

The photopolymer layer was then simultaneously exposed and probed using the setup shown in Fig. 4, until bleaching of the layer took place. Spatially filtered and collimated laser beams were used and the transmitted power of both the exposing and the probing laser beam were measured simultaneously. The duration of the exposures was controlled using an electronic shutter. The green exposing beam passes through an iris of diameter 0.56 cm giving an exposed area of 0.25 cm^2. The exposing beam is normally incident on the photopolymer layer. The probing beam, limited by an iris of diameter 0.4 cm, passed through the exposed photopolymer area at an angle of $\sim 20°$ to the normal in air, i.e., $\theta \sim 13°$ inside the layer.

Having described the experimental method and setup, we now proceed to process the experimental results for both beams and different exposing intensities, in order to estimate key parameter values.

V. EXPERIMENTAL RESULTS AND THE ESTIMATED PARAMETER VALUES

The experiments were performed using the material described in Sec. II and the setup described in Sec. IV. Three figures, containing both the exposing and probing transmission curves (Figs. 5–7) for three exposing intensities (16, 32, and 132 mW/cm^2), including error bars to indicate experimental reproducibility, are presented. In all figures both the exposing and probe transmissions are normalized and are plotted as functions of the exposing time in seconds. These transmission curves were fitted using Eqs. (9) and (10).

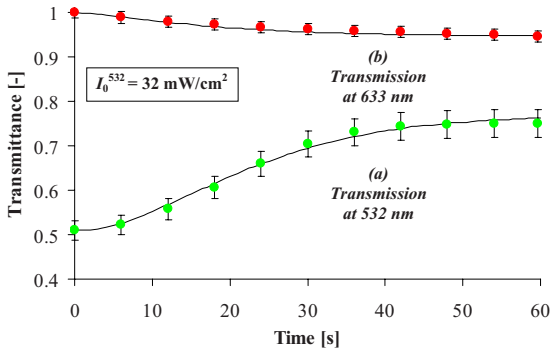

FIG. 6. (Color online) Experimental data (dots) and theoretical fits (solid line) to (a) green and (b) red transmittance data. The intensity of the green exposing beam is 32 mW/cm^2.

Numerical fitting was performed by searching for the minimum deviation of the experimentally measured normalized transmitted exposing intensity curves, $T_{\text{data}}^{532}(t)$, from those predicted by the model presented in Sec. IV, $T_{\text{fit}}^{532}(t)$. The RMSE function at the exposing wavelength $\lambda = 532$ nm, RMSE^{532}, is used as the cost function to evaluate the quality of fits to these data.

$$\text{RMSE}^{\lambda} = \frac{1}{N}\sqrt{\sum_{i=1}^{N}[T_{\text{fit}}^{\lambda}(t_i) - T_{\text{data}}^{\lambda}(t_i)]^2}, \tag{11}$$

where T_{fit}^{λ} is the value predicted by the model at a particular time t_i and wavelength λ nm, $T_{\text{data}}^{\lambda}$ is the corresponding measured data, and N is the number of discrete samples used.

To perform this fitting, the rate constants, k_{iso}, k_Z, k_B, and k_C and the molar absorption coefficients $\varepsilon_{A^*}^{532}$ and ε_B^{532} are iteratively searched for over predefined search ranges in order to find a minimum RMSE^{532} value. The search ranges used are listed in Table II, and we discuss how these were identified later in this section. The rate constant of reverse isomerization k_{riso} is assumed to be negligible over the period of exposure examined in this paper, when compared to the other rate constants involved in the initiation processes; i.e., $k_{\text{riso}} \ll k_{\text{iso}}$.

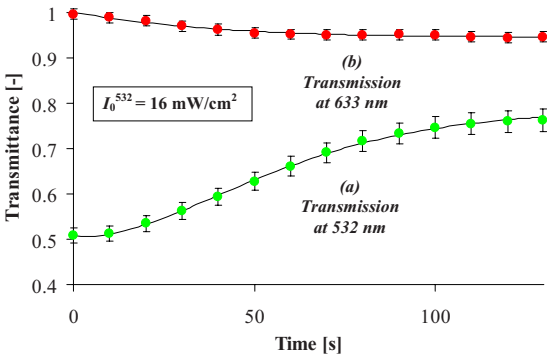

FIG. 5. (Color online) Experimental data (dots) and theoretical fits (solid line) to (a) green (532 nm) and (b) red (633 nm) transmittance data. The intensity of the green exposing beam is 16 mW/cm^2.

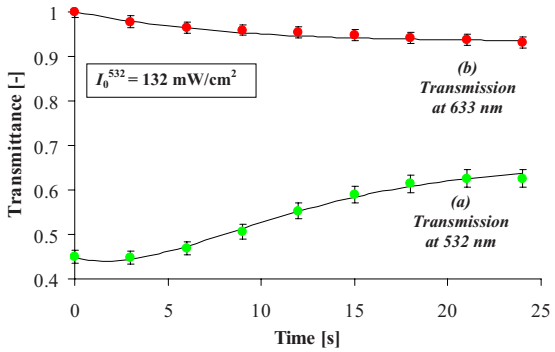

FIG. 7. (Color online) Experimental data (dots) and theoretical fits (solid line) to (a) green and (b) red transmittance data. The intensity of the green exposing beam is 132 mW/cm^2.

TABLE II. Parameters extracted by fitting both the red and the green transmission curves simultaneously.

I_0^{532} (mW cm^{-2}) (figure)	d (mm)	$Z(0)$ (mol cm^{-3}) ($\times 10^{-7}$)	k_z (cm^3/mol s) ($\times 10^8$)	k_{iso} (cm^3/ Einstein s) ($\times 10^4$)	k_B (s^{-1}) ($\times 10^{-2}$)	k_C (s^{-1}) ($\times 10^{-2}$)	$\varepsilon_{A^*}^{532}$ cm^2/ mol) ($\times 10^5$)	$\varepsilon_{A^*}^{633}$ cm^2/ mol) ($\times 10^4$)	ε_B^{633} cm^2/ mol) ($\times 10^4$)	ε_B^{532} cm^2/ mol) ($\times 10^4$)	RMSE (—) λ=532 nm ($\times 10^{-4}$)	RMSE (—) λ=633 nm ($\times 10^{-4}$)
16 (Fig. 5)	0.45	3.8	1.1	39.44	2.41	1.25	1.36	0.84	1.7	4.59	23	23
32 (Fig. 6)	0.45	3.8	1.1	39.00	9.7	3.53	1.46	0.60	1.5	4.83	56	85
132 (Fig. 7)	0.55	3.6	1.1	39.00	11.73	4.19	1.53	0.70	1.6	7.49	47	27
Search range	⋯	1–10	0.01–10	30–60	1–12	1–10	1.3–1.6	0.3–1	0.3–2	3–9	—	—

Fits are then made to the corresponding probing transmission curves using the extracted values for the rate constants and molar absorption coefficients estimated during the previous exposing beam fitting procedure. Then the same iterative procedure is employed but using RMSE^{633} as the cost function. The resulting fits, for both transmittance curves, are presented as solid lines in Figs. 5–7 with the associated experimental error bars.

We now describe the fitting algorithm in more detail. In order to extract the parameter values we first fix $\varepsilon_A^{532}=1.2\times10^5$ cm^2/mol, which is found from the absorption spectrum in Ref. 17. We note that this value is consistent with our results. The initial photoinitiator concentration $A(0)=1.04\times10^{-4}$ mol/cm^3, and the initial photoproduct concentrations are $A^*(0)=B(0)=C(0)=0$. The photopolymer layer thickness is known from measurements to be ~0.5 mm. However, we note that to reproduce a uniform consistent thickness is difficult. Although significant efforts were made to produce uniform layers, both spacers and substrate thickness variations, and shrinkage during curing can produce a measured worst case thickness variation of up to 15% between different samples produced in house.

Two complementary methods were employed to measure layer thickness. (1) Total sample thickness postrecording were measured by a micrometer screw gauge. Then by subtracting average values of the glass substrate and cover plate thicknesses the material layer thickness could be estimated. (2) Another method used to estimate the layer thickness was by using the initial transmittance value $T^{532}(0)$, which can be determined if $A(0)$ and ε_A^{532} are known. However, this method assumes that the optical quality across the plate is constant, which was not always the case. In Table II, the thicknesses presented were estimated using method (1). The remaining parameters are then obtained using the fitting procedure described above.

The parameter search ranges used are also provided in Table II. We assume that the reducing agent present in the photopolymer is a combination of two chemicals: (i) dissolved oxygen, which is well known to act as a quencher in photopolymer materials,[5,7,13,19,21] and (ii) the inhibitor, BHT,[5] i.e., $Z(0)=Z_{\text{BHT}}(0)+Z_{\text{O}_2}(0)$. The initial concentration of BHT included in the material composition (see Sec. II) is $Z_{\text{BHT}}(0)=2.8\times10^{-6}$ mol/cm^3. Concentrations of dissolved oxygen, found in other photopolymer materials, are of the order of 10^{-6}–10^{-7} mol/cm^3.[6,24] Therefore $Z(0)$ is searched for in the range 10^{-6}–10^{-7} mol/cm^3. The associated reaction rate k_Z governing the reaction between Z and **B** is therefore expected to be a combination of the rate reaction of the **B** intermediate product reacting with BHT and the dissolved oxygen, respectively. The rate of reaction of the dissolved oxygen with the initiating species (**B** in our case) is expected to be relatively very fast, i.e., of order 10^9 mol^{-1} cm^3 s^{-1}.[6] The reaction of the inhibitor with the photocleaved radicals is reported as proceeding at a high reaction rate.[5] We therefore also assume that the reaction of **B** and BHT occurs at a high rate, and our search range for k_Z is 10^6–10^9 mol^{-1} cm^3 s^{-1}. The rate of removal of **A**, and of the production of **A***, k_{iso}, is related to ε_A^{532} and the quantum yield of photoinitiator removal.[25] Therefore a search range of $k_{\text{iso}}\in 3\times10^4$–$6\times10^4$ cm^3 Einstein^{-1} s^{-1} appears reasonable. The reaction rates for photocleaving (creating **B**), k_B, and the direct production of **C**, k_C, are both searched for in order to produce good fits to both the exposing and probe beam experimental transmission curves. The values of these two rates depend on $\varepsilon_{A^*}^{532}$ and ε_B^{532}. As discussed in Secs. IV B and IV C, we expect that $\varepsilon_{A^*}^{532}>\varepsilon_A^{532}$; therefore our search range for $\varepsilon_{A^*}^{532}$ is assumed to be 1.3×10^5–1.5×10^5 cm^2/mol. It is also assumed that $\varepsilon_A^{532}>\varepsilon_B^{532}$, which is reasonable, based on the shape and maximum value of our experimental transmission curves. If this were not the case, photoinitiator removal would proceed slowly with a much flatter transmission curve (a lesser slope). Therefore ε_B^{532} is searched for in the range 3×10^4–9×10^4 cm^2/mol. Combining these assumptions constrains our search to the ranges 10^{-2}–10^{-1} s^{-1} for both k_B and k_C. The search for $\varepsilon_{A^*}^{633}$ and ε_B^{633} only takes place after all the other exposing parameters have been extracted. It is found that these parameters control the initial slope and saturation transmission value of the probing transmission curve. Suitable search ranges have been identified to be $\varepsilon_{A^*}^{633}\in 3\times10^3$–$10^4$ cm^2/mol and $\varepsilon_B^{633}\in 7\times10^3$–$2\times10^4$ cm^2/mol.

Returning to Figs. 5–7 we note that the transmitted probe intensities decrease with increasing exposing intensity. This may be the result of a more complex photochemical reaction mechanism taking place, rather than the assumed processes presented in Sec. III; e.g., the isomer may not form a transparent state directly, but may react to form absorptive intermediate species before reaching the stable transparent state, **C**. In Fig. 7, for the highest exposing intensity, i.e., 132 mW/cm^2, the exposing transmission curve has a lower saturation value (<10%) than for the 16 and 32 mW/cm^2 exposing intensity cases. Once again the reason for this could be due to the assumption that the isomer may not form

a transparent state directly. The largest decrease in the transmitted probe beam intensity is also observed for the highest intensity case. This is consistent with the assumed initiator processes presented in Sec. III; i.e., that a larger accumulation of absorptive intermediates are more rapidly produced for higher exposing intensities.

By applying our model, in conjunction with numerical fitting techniques, estimates were obtained for the reaction rates, k_Z, k_{iso}, k_B, and k_C, and molar absorption coefficients, $\varepsilon_{A^*}^{532}$, $\varepsilon_{A^*}^{633}$, ε_B^{532}, and ε_B^{633}, from fits to reproducible experimental transmission curve data and are presented in Table II. All the extracted parameter values lie within physically reasonable ranges as presented in the literature.

VI. CONCLUSIONS

In this paper we have reported a physical model describing the behavior of Irgacure 784 photoinitiator in a photopolymer layer composed of an epoxy resin matrix and vinyl monomers. In deriving this model we have assumed that two absorptive photoproducts are generated during photoinitiation. Photochemical rate equations were derived, which describe the removal, through absorption, of the Irgacure 784 and the production of these photoproducts. In order to quantify the effects of the photoproducts, an experimental setup was developed, involving simultaneous measurements of the light transmitted at two different wavelengths. The resulting data are used to perform the necessary absorptive and photoinitiating studies.

We report results for experiments carried out at three different exposing intensities. Both the probe and the exposing beam transmission curves are optimally fitted using the developed material model, by searching for the lowest RMSE cost function values possible. Such iterative searches, constrained to take place over physical parameter ranges, can be used to estimate values of the rate constants and molar absorption coefficients, since direct measurements of these values are difficult to perform *in situ*. From our experimental data we are able to estimate an *absorbance* or *optical density*, i.e., the molar absorption multiplied by the absorber's concentration. Based solely on measurements of the transmittance of the exposing light, we cannot simply estimate the concentrations of the absorber, **B** product, and the final transparent, **C** product. However, by applying our model, in conjunction with an iterative search procedure, we have successfully predicted the experimentally observed behavior and estimated these parameters.

In the future we aim to (i) improve the photoinitiator model further to allow for the more complex multiabsorber environment, which appears to be indicated by our experimental results, and (ii) use our better understanding of the photoinitiation photochemistry of Irgacure 784, in order to more accurately predict free radical production. This will lead to the incorporation of more accurate photoinitiation models, which can then be included into the nonlocal photopolymerization diffusion driven model,[6,11] enhancing our ability to analyze holographic formation[26] and the beam writing of polymer waveguides[27] in such materials.

ACKNOWLEDGMENTS

We acknowledge the financial support of Enterprise Ireland, Science Foundation Ireland, and the Irish Research Council for Science, Engineering and Technology under the National Development Plan.

[1] H. J. Coufal, D. Psaltis, and G. T. Sincerbox, *Holographic Data Storage, Springer Series in Optical Sciences* (Springer, Berlin, 2000).
[2] M. D. Goodner and C. N. Bowman, Chem. Eng. Sci. **57**, 887 (2002).
[3] B. Klingert, M. Riediker, and A. Roloff, Comments Inorg. Chem. **7**, 109 (1988).
[4] H. Curtis, E. Irving, and B. F. G. Johnson, Chem. Br. **22**, 327 (1986).
[5] M. R. Gleeson, "Analysis of the photochemical kinetics in photopolymers for holographic data storage and hybrid photonics circuits," Ph.D. thesis, University College Dublin, 2008.
[6] M. R. Gleeson, D. Sabol, S. Liu, C. E. Close, J. V. Kelly, and J. T. Sheridan, J. Opt. Soc. Am. B **25**, 396 (2008).
[7] M. R. Gleeson, S. Liu, S. O'Duill, J. T. Sheridan, J. Appl. Phys. **104**, 064917 (2008).
[8] T. J. Trentler, J. E. Boyd, and V. L. Colvin, Chem. Mater. **12**, 1431 (2000).
[9] L. V. Natarajan, D. P. Brown, J. W. Wofford, V. P. Tondiglia, R. L. Sutherland, P. F. Lloyd, and T. J. Bunning, Polymer **47**, 4411 (2006).
[10] S. H. Lin, Y.-N. Hsiao, and K. Y. Hsu, J. Opt. A, Pure Appl. Opt. **11**, 024012 (2009).
[11] M. R. Gleeson and J. T. Sheridan, J. Opt. Soc. Am. B **25**, 1736 (2009).
[12] M. R. Gleeson, J. T. Sheridan, J. Opt. Soc. Am. B **25**, 1746 (2009).
[13] G. Odian, *Principles of Polymerization* (Wiley, New York, 1991).
[14] J. Jakubiak and J. F. Rabek, Polimery **44**, 447 (1999).
[15] M. C. Cole, F. R. Aksham, and W. L. Wilson, U.S. Patent No. 2006/0194120 A1 (31 August 2006).
[16] N. Davidenko, O. Garcia, and R. Sastre, J. Biomater. Sci., Polym. Ed. **14**, 733 (2003).
[17] M. Degirmenci, A. Onen, Y. Yagci, and S. P. Pappas, Polym. Bull. (Berlin) **46**, 443 (2001).
[18] U. Zucchini, E. Albizzati, and U. Giannini, J. Organomet. Chem. **26**, 357 (1971).
[19] B. Klingert and A. Roloff, Helv. Chim. Acta **71**, 1858 (1988).
[20] K. Meier, Coord. Chem. Rev. **111**, 97 (1991).
[21] S. Liu, M. R. Gleeson, and J. T. Sheridan, J. Opt. Soc. Am. B **26**, 528 (2009).
[22] S. Liu, M. R. Gleeson, D. Sabol, and J. T. Sheridan, Proc. SPIE **7358**, 73580Q (2009).
[23] M. W. Grabowski, K. M. Vogelhuber, D. Sabol, J. H. Chen, R. R. McLeod, and J. T. Sheridan, Proc. SPIE **7053**, 70530D (2008).
[24] M. R. Gleeson, J. V. Kelly, D. Sabol, C. E. Close, S. Liu, J. T. Sheridan, J. Appl. Phys. **102**, 023108 (2007).
[25] G. A. Miller, L. Gou, V. Narayanan, and A. B. Scanton, J. Polym. Sci., Part A: Polym. Chem. **40**, 793 (2002).
[26] J. T. Sheridan, M. R. Gleeson, and J. V. Kelly, J. Nanosci. Nanotechnol. **7**, 1 (2007).
[27] A. C. Sullivan, M. W. Grabowski, and R. R. McLeod, Appl. Opt. **46**, 295 (2007).